tvst

Article

Correlation Between Laser Speckle Flowgraphy and OCT-Derived Retinal and Choroidal Metrics in Healthy Human Eye

Yiming Lu[1], Hao Zhou[1], Xiao Zhou[1], Yuxuan Chen[1], and Ruikang K. Wang[1,2]

[1] Department of Bioengineering, University of Washington, Seattle, WA, USA
[2] Karalis Johnson Retina Center, Department of Ophthalmology, University of Washington, Seattle, WA, USA

Correspondence: Ruikang K. Wang, 3720 15th Avenue NE, Seattle, WA 98195, USA. e-mail: wangrk@uw.edu

Received: February 11, 2022
Accepted: May 17, 2022
Published: June 15, 2022

Keywords: laser speckle flowgraphy; optical coherence tomography; optical coherence tomography angiography; retina; choroid

Citation: Lu Y, Zhou H, Zhou X, Chen Y, Wang RK. Correlation between laser speckle flowgraphy and OCT-derived retinal and choroidal metrics in healthy human eye. Transl Vis Sci Technol. 2022;11(6):15, https://doi.org/10.1167/tvst.11.6.15

Purpose: To investigate the correlation between laser speckle flowgraphy (LSFG) signals and the quantitative metrics derived from optical coherence tomography (OCT) in normal eyes.

Methods: LSFG, OCT, and OCT angiography (OCTA) imaging were performed on normal participants using a custom-designed LSFG system and a commercial swept-source OCT system. Mean (PWM) and amplitude (PWA) of the LSFG pulse waveform were selected to quantify the LSFG signals. Retinal and choroidal maps were obtained using the standard 6 × 6 mm OCT and OCTA scans. Structural and vascular metrics maps, including thickness, vessel area density, vessel skeleton density, and vessel diameter index of the retina, and choroidal thickness (CT), choroidal vessel volume (CVV) and choroidal vessel index (CVI), were employed to quantify the retinal and choroidal properties. Correlation analysis was then performed between the LSFG, retinal, and choroidal metrics maps.

Results: Twelve healthy participants aged 23 to 36 years were enrolled in this study. The spatial distribution of the PWM and PWA values was highly correlated with that of the CT and CVV metrics. On average, Spearman correlation coefficients (ρ) were 0.80 and 0.78 (all $P < 0.001$) for the correlations between PWM and CT and CVV, respectively, and were 0.61 and 0.63 (all $P < 0.05$) for the correlations between PWA and CT and CVV, respectively. In comparison, both PWM and PWA were generally weak or not correlated with all the retinal metrics and CVI.

Conclusions: LSFG signals were positively correlated with the choroidal thickness and vessel volume, suggesting choroidal blood flows dominate the LSFG signals at the area absent of large retinal vessels.

Translational Relevance: This study illustrates the dominant source of the LSFG signals in the eye.

Introduction

Choroid is a vascular layer lying between the retina and sclera of the eye. The blood perfusion in the choroid is critical for maintaining the normal vision as it supports the metabolic exchange between the circulations of the retinal pigment epithelium (RPE) and photoreceptors.[1,2] Abnormal choroidal blood perfusion is observed in eye diseases, such as diabetic retinopathy (DR), age-related macular degeneration (AMD), and glaucoma, using fluorescein angiography (FA) and indocyanine green angiography (ICGA).[3–5] However, the need for dye injections in FA and ICGA impedes their applications for routine clinical monitoring.

Laser speckle flowgraphy (LSFG) is a noninvasive and dye-free imaging technique that employs the laser speckle statistics to assess the blood flow.[6,7] It has been shown useful in the investigations of blood flows in the retina, optical nerve head (ONH), and choroid.[7–9] Abnormal LSFG signals were observed in prevalent eye diseases, including DR, AMD, and glaucoma.[10–12] Currently, most of the ophthalmic

LSFG techniques use near-infrared lasers as the light source, and LSFG is a two-dimensional spatial imaging technique.[6,7,13] Therefore, LSFG signals emerging from the eye are an accumulation of the signals from the retinal and choroidal layers. The dominant source of the LSFG signals can only be determined at the locations where retinal and choroidal vessels are distinct.[9,14] Moreover, spatial resolution in LSFG imaging is relatively low, making small vessels in the retina and choroid generally unresolvable. Therefore, it is still not well clarified how retinal and choroidal blood flows contribute to the LSFG signals at the locations where the retinal and choroidal vessels cannot be clearly resolved, impeding the investigations of the involvement of choroidal blood perfusion in disease development. Previous LSFG studies of choroidal blood perfusion mostly focused on single large choroidal vessels or were centered at the fovea region to minimize the contamination from retinal perfusions.[9,15–17]

Optical coherence tomography (OCT) and OCT angiography (OCTA) have been widely used in the imaging of retinal structure and vasculature. OCTA of the retina provides visualization of the retinal vasculatures, including capillaries, with high spatial resolution, enabling accurate quantification of the vascular characteristics.[18–21] However, OCT and OCTA imaging of the choroid has been challenging due to the strong scattering and absorption of light by the RPE and choroid. The development of swept-source OCT (SSOCT) enables deeper penetration and has less sensitivity roll-off compared with the conventional spectrum-domain OCT. Therefore, SSOCT provides a better visualization of the choroid.[22,23] Using SSOCT, choroidal thickness changes were observed in eye diseases, including DR, AMD, and glaucoma.[24–26] Recently, an attenuation correction-based technique was suggested to correct the attenuation on SSOCT structural scans, which was shown to improve the imaging of choroid.[27,28] It works to compensate the OCT signal for the attenuation of light along each A-scan to enhance the contrast of choroidal vessels and stroma. This compensation makes it possible to accurately segment the choroid and provide unambiguous visualization and measurement of the choroidal vasculatures.

The depth-resolved capability of OCT and OCTA enables independent extraction of the retinal and choroidal vasculatures, promising an alternative method to clarify the dominant source of the LSFG signals in the eye. At the regions where blood vessels cannot be resolved in the LSFG map, accurate vasculature information of the retinal and choroidal slabs can be retrieved using OCT and OCTA instead. As LSFG signals reflect the blood flows in the tissue, comparing the properties of the LSFG signals and the retinal and choroidal vasculatures, respectively, can provide references about the dominant source of the LSFG signals. Therefore, in this study, we investigated the LSFG signals at the regions in the LSFG map where retinal vessels cannot be resolved, with the assistance of OCT and OCTA. Specifically, these regions, termed the background region in this study, consist of retinal capillaries and nonvascular tissue and choroidal vessels and stroma. OCTA and attenuation-corrected OCT were employed to image the retinal and choroidal structure and vasculature.[27,29] Multiple metrics maps about the retina and choroid were then derived for quantitative analysis.[19] Topographic correlations between the LSFG signals and the retinal and choroidal metrics were established to reveal the source of the LSFG signals.

Methods

Participants without any known ocular diseases were recruited for this study. All the participants underwent both OCT and LSFG imaging of their right eyes consecutively. All the experiments were conducted in an environment with minimum ambient light and without using pharmacologic pupil dilation. The use of commercial OCT and LSFG prototype devices for imaging human participants was approved by the Institutional Review Board of the University of Washington, and the protocols adhered to the tenets of the Declaration of Helsinki. Informed written consents were obtained from all the participants involved in this study.

LSFG imaging was performed by using a custom-designed imaging system that has been described previously.[30] In brief, the system employed a light source with a wavelength at 785 nm and had an imaging speed of 80 frames/s with an exposure time of 5 ms for each frame. It is known that blood flow alters the local light field and decorrelates the laser speckles over time at the vessel area where there are moving blood cells (i.e., blood flow). The decorrelation rate of the laser speckles is correlated with the blood flow.[31] Therefore, in this study, we used the mean decorrelation rate to indicate the blood flow in the LSFG maps. The raw laser speckle fundus images were processed by a spatiotemporal algorithm to calculate the mean decorrelation rate and generate the LSFG images.[30] The field of view was chosen to center at the posterior pole of the eye to cover most of the fovea and the perifovea region between the fovea and ONH.

A commercial swept-source OCT system (PLEX Elite 9000; Carl Zeiss Meditec, Inc., Dublin, CA, USA) was used for the OCT and OCTA imaging. The system employed a 100-kHz swept-source laser (100,000 A-lines/s) with a central wavelength at 1060 nm and a bandwidth of 100 nm. A standard 6 × 6 mm scanning protocol, which contained 500 B-scans and 500 A-lines/B scan, was used in this study. The retinal layers were automatically segmented by the built-in algorithm of the system and further manually verified by experienced readers. The output 6-mm × 6-mm OCTA image of retina was a projection of the retinal vessels between the internal limiting membrane (ILM) and an offset of ~99 µm above Bruch's membrane (BM) (i.e., the definition of the whole retinal slab in the commercial OCT system) to minimize the hyperreflection from RPE (Figs. 1A, 1B). Large blood vessels in the retinal OCTA image were identified using a custom-designed algorithm with an empirical threshold.[32] As OCTA and LSFG are of different spatial resolution, the identified vessel regions were further dilated by ~60 µm to fully cover the corresponding retinal vessels in the LSFG. The large vessel areas were then removed from the retinal OCTA image to minimize the contribution of large vessels to the quantification of the retinal capillaries (Fig. 1C). The ONH region was also manually excluded to avoid artifacts.

After removing the large retinal vessels and ONH, three spatially resolved measurements were retrieved from the retinal OCTA image to quantify the spatial characteristics of the retinal capillaries[19]: (1) vessel area density, which measured the proportion of the blood vessel area relative to the total area at a local region; (2) vessel skeleton density, which measured the ratio of the blood vessel length relative to the total area at a local region; and (3) vessel diameter index, which measured the ratio of the blood vessel area relative to the blood vessel length at a local region. The retinal thickness map, which measured the distance between the ILM and BM, was also obtained for this study.

Three measurements of choroid (i.e., choroidal thickness [CT], choroidal vessel volume [CVV], and choroidal vessel index [CVI]) were obtained from the OCT data sets using a previously described method.[27,28] This method used light attenuation correction to enhance the choroidal structures and then used the inverted OCT structure scans to delineate the choroidal vasculatures (Fig. 1D). CT measured

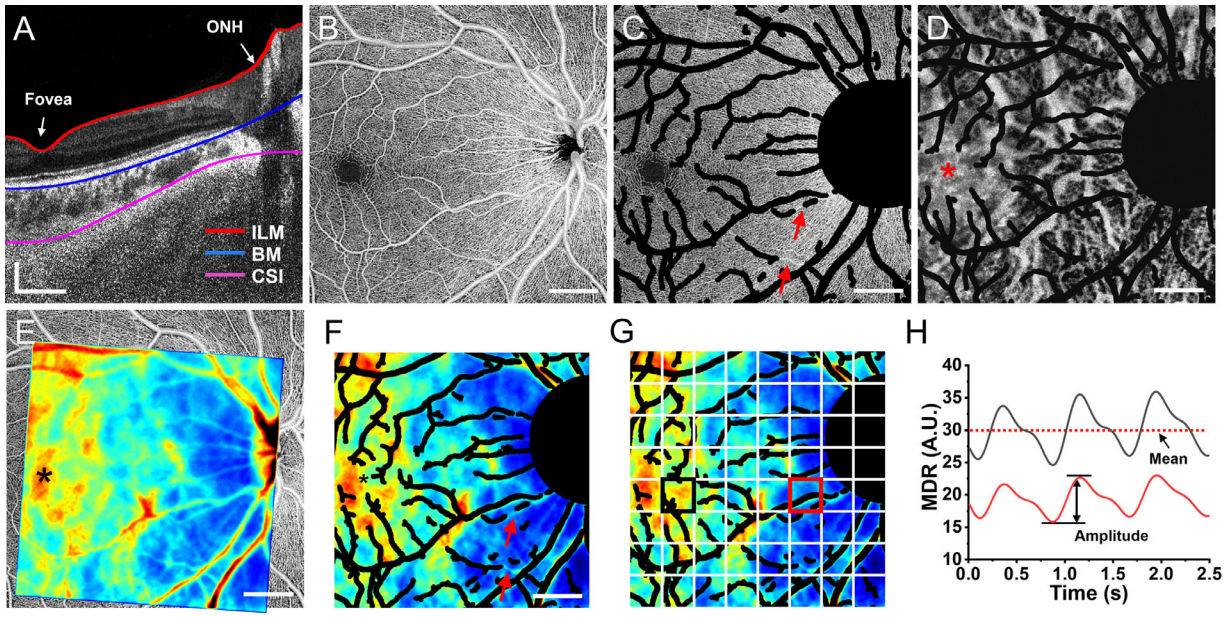

Figure 1. (A) Representative OCT B-scan after attenuation correction and the corresponding segmentations of the ILM, BM, and choroidal–scleral interface layers. (B) Representative 6-mm × 6-mm OCTA map of retina generated by the commercial OCT system. (C) Same OCTA map of retina as in (B) but with large retinal vessels and the ONH region removed (*black areas*). (D) Representative choroidal vasculature map generated from the attenuation-corrected OCT choroid slab as shown in (A). The *black areas* indicate the large retinal blood vessels and ONH region were eliminated from the choroidal data. (E) Overlay of retinal OCTA and LSFG maps after image registration. (F) LSFG map of the ROI with the large retinal blood vessels and ONH region eliminated (*black areas*). (G) The ROI was separated into 8 × 8 subregions to facilitate the topographic correlation study. (H) Representative pulse waveforms of LSFG. The *black* and *red* waveforms show the averaged signals from the subregions indicated by *black* and *red rectangles* in (G), respectively. MDR, mean decorrelation rate. *Red arrowheads* in (C) and (F) show portions of large retinal vessels that were not identified. *Asterisks* in (D–F) show the location of fovea. *Vertical* and *horizontal scale bars* represent 200 µm and 1 mm, respectively.

the thickness of the choroid slab from the BM to the choroidal–scleral interface (Fig. 1A). CVV measured the volume of choroidal vessels. CVI measured the choroidal vessel density, which is the ratio of CVV and the total volume of the choroidal slab. The areas corresponded to the large retinal vessels, and ONH in the retinal OCTA map was removed from the CT, CVI, and CVV maps for the correlation study.

The LSFG images were registered with the retinal OCTA image using a rigid registration algorithm (MATLAB; MathWorks, Natick, MA, USA) (Fig. 1E). The overlapped region of the registered LSFG and retinal OCTA image was determined as the region of interest (ROI) in the eye. As shown in Figure 1F, the areas in the LSFG images that corresponded to the large retinal blood vessels and ONH region were excluded from calculation using the blood vessel and ONH masks obtained from the retinal OCTA image (Fig. 1C). The ROI was then separated into multiple subregions in all LSFG, retinal, and choroidal metrics maps to investigate the spatial correlations between the LSFG signals and the retinal and choroidal vasculature metrics. As shown in Figure 1G, the ROI was separated into 8×8 subregions in this study. The grid was applied to the LSFG, retinal, and choroidal metrics maps. The data within each subregion were averaged and used for the correlation study. Such selection was a compromise between reducing image difference correlated with different imaging modalities and obtaining reasonable spatial sampling points for the correlation study.

Pulse waveform of LSFG was generated for each subregion. Two parameters, mean and amplitude of the pulse waveform, were selected to represent the LSFG characteristics and were used for quantitative analysis (Fig. 1H). The mean of the pulse waveform (PWM) was defined as the average of all signals within the specified subregion over the whole acquisition period. The amplitude of the pulse waveform (PWA) was defined as the difference between averaged peak and trough values of the waveform. Therefore, PWM reflects the total blood flow and PWA correlates with the difference between systolic and diastolic pressure.

Spearman's correlation analysis was employed to evaluate the correlations between the topography of the LSFG, retinal, and choroidal metrics. Spearman's correlation was selected with the consideration that the metrics were affected by the natural attributes of the vessels and therefore were not necessarily normally distributed. Significant correlations were determined as the absolute value of Spearman's correlation coefficient $|\rho| > 0.5$ and $P < 0.05$.

Results

A total of 12 right eyes from 12 normal participants (age range: 23–36 years; 7 females, 5 males) were imaged in this study. The ROIs were either centered at the perifovea area between the fovea and ONH with most of the fovea covered or centered at the fovea. Figure 2 shows LSFG, retinal, and choroidal metrics maps obtained from a representative participant. As shown in Figure 2A, the ROI was centered at the perifovea between the fovea and ONH and covered

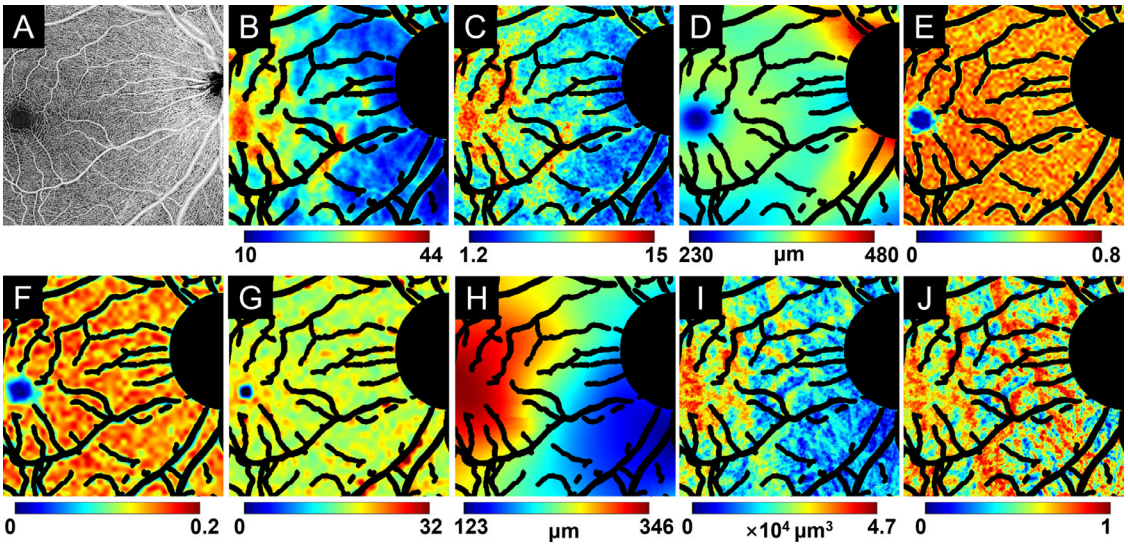

Figure 2. Representative maps of LSFG, retinal, and choroidal measurements with ROI centered at the perifovea. (A) Retinal OCTA map of the ROI. (B) PWM and (C) PWA map of LSFG. (D–G) Retinal thickness (RT) map, vessel area density (VAD) map, vessel skeleton density (VSD) map, and vessel diameter index (VDI) map of the retina. (H–J) CT map, CVV map, and CVI map. The regions correspond to the large blood vessels, and ONH was removed from measurements.

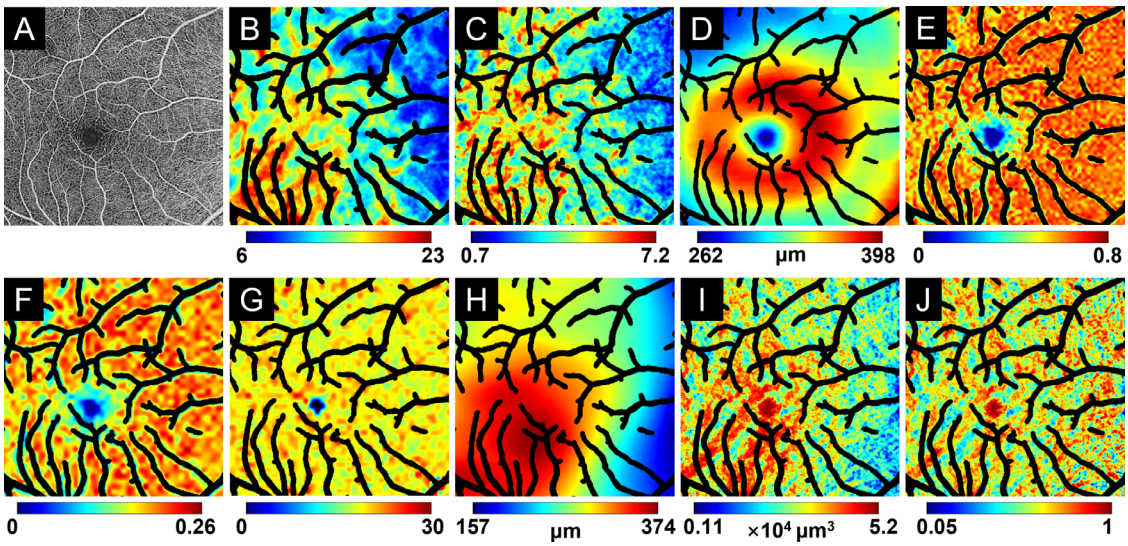

Figure 3. Representative maps of LSFG, retinal, and choroidal measurements with ROI centered at the fovea. (A) Retinal OCTA map of the ROI. (B) PWM and (C) PWA map of LSFG. (D–G) RT, VAD, VSD, and VDI maps of the retina. The regions correspond to the large blood vessels, and ONH as removed from measurements. (H–J) CT, CVV, and CVI map.

most part of the fovea. Figures 2B and 2C show the PWM and PWA maps of the LSFG, respectively, in which the foveal region (temporal part of Figs. 2B, 2C) presented higher values compared to the regions close to the ONH. However, the retinal metrics maps were relatively more homogeneous except the foveal avascular zone (FAZ), where retinal thickness is thinner, and the retinal vessels are absent (Figs. 2D–G). In comparison, the values were generally higher at the fovea in the CT and CVV maps, which was in accordance with the LSFG maps (Figs. 2H, 2I). The CVI map showed higher values at the choroidal vascular regions, but it did not significantly differ in the foveal region from other regions of the ROI (Fig. 2J).

Figure 3 shows a representative comparison of the LSFG, retinal, and choroidal metrics obtained from a different participant with the ROI centered near the fovea (Fig. 3A). In this case, the PWM and PWA maps of LSFG exhibited higher values at the temporal-inferior region of the ROI (Figs. 3B, 3C). As shown in Figures 3D–G, the retinal metrics maps presented minimum values at the FAZ and generally homogeneous values around the FAZ, which was significantly different from the LSFG metrics maps. CT and CVV maps were similar to the PWM and PWA maps in the aspect that the values were also generally higher at the temporal-inferior part of the ROI (Figs. 3H, 3I). There was also no significant accordance between the LSFG maps and CVI maps (Figs. 3B, 3C, 3J).

To quantitatively assess the spatial correlations between the LSFG and the retinal and choroidal metrics derived from OCT, the ROI was separated into 64 subregions using a grid illustrated in the Methods section (Fig. 1G). Mean value of the data was obtained for each subregion, and Spearman's correlation analysis was applied to all the mean values. Representative correlation analysis of the participant shown in Figure 2 is illustrated in Figures 4 and 5. In accordance with the observations in Figures 2 and 3, LSFG PWM was not or weakly correlated with the retinal metrics as all the values of Spearman's correlation coefficients (ρ) were between -0.2149 and 0.3892 (Figs. 4A–D). In comparison, the PWM was significantly correlated with the CT ($\rho = 0.8482$, $P < 0.0001$) and CVV ($\rho = 0.8355$, $P < 0.0001$) (Figs. 4E, 4F). The PWM was also weakly correlated with the CVI ($\rho = 0.2671$) (Fig. 4G).

The results are similar for the correlations between the PWA of LSFG and the retinal and choroidal metrics (Fig. 5). PWA was not or weakly correlated with the retinal metrics ($-0.2309 < \rho < 0.3874$) (Figs. 5A–D). PWA was also significantly correlated with CT ($\rho = 0.8714$, $P < 0.0001$) and CVV ($\rho = 0.8422$, $P < 0.0001$) but not correlated with CVI ($\rho = 0.2370$, $P = 0.0659$) (Figs. 5E–G).

Correlation analysis results from 12 normal participants are shown in Figures 6 and 7. Data were plotted in a manner of Spearman's correlation coefficient against the corresponding P value. In the correlations between PWM and the OCT-derived retinal metrics, most of Spearman's correlation coefficients had a value between -0.5 and 0.5, and the corresponding P values were generally larger than 0.05 (Figs. 6A–D). On the other hand, all correlation

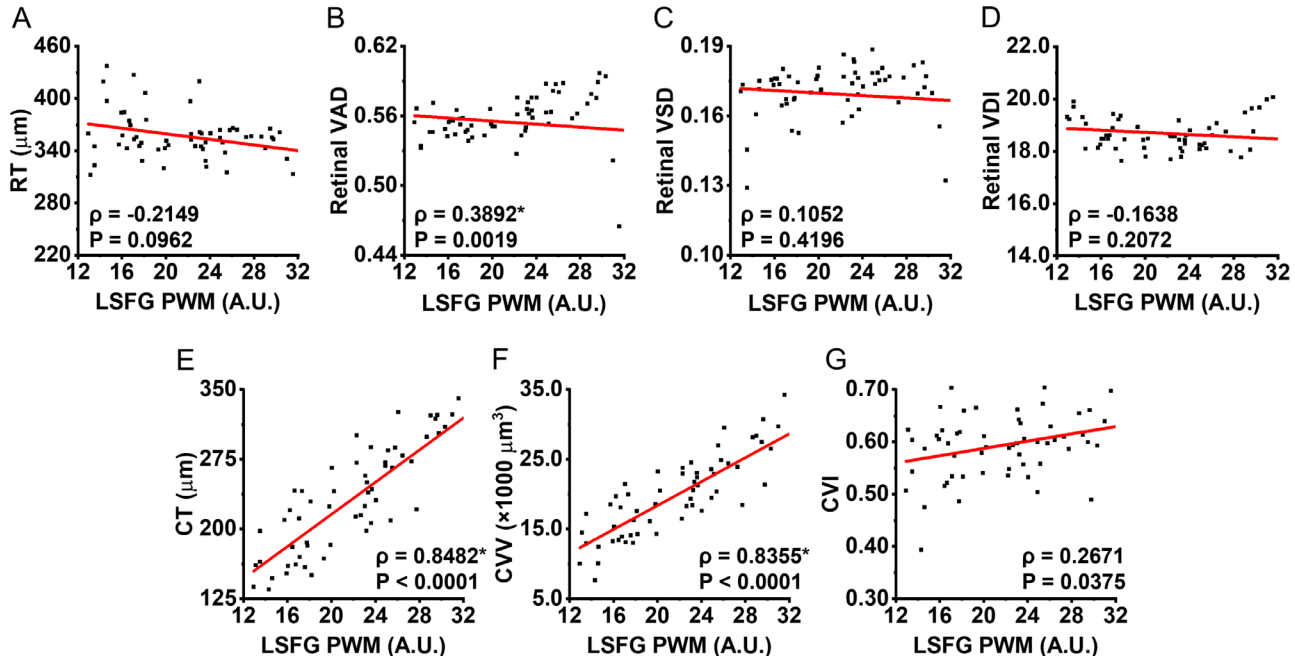

Figure 4. Representative correlations between the mean value of the LSFG PWM and the OCT retinal and choroidal metrics. (A–D) Correlations between PWM and RT, VAD, VSD, and VDI. (E–G) Correlations between PWM and CT, CVV, and CVI. The *red lines* represent the linear fitting of the scatters in each plot. Data were analyzed through Spearman's correlation analysis. Significance level was determined as $P < 0.05$.

coefficient values were larger than 0.5, and the corresponding P values were all smaller than 0.01 for the correlations between PWM and CT and CVV (Figs. 6E, 6F). The correlation between PWM and CVI was also weak and generally not significant, and correlation coefficient values were distributed between −0.5 and 0.5, with most P values larger than 0.05 (Fig. 6G).

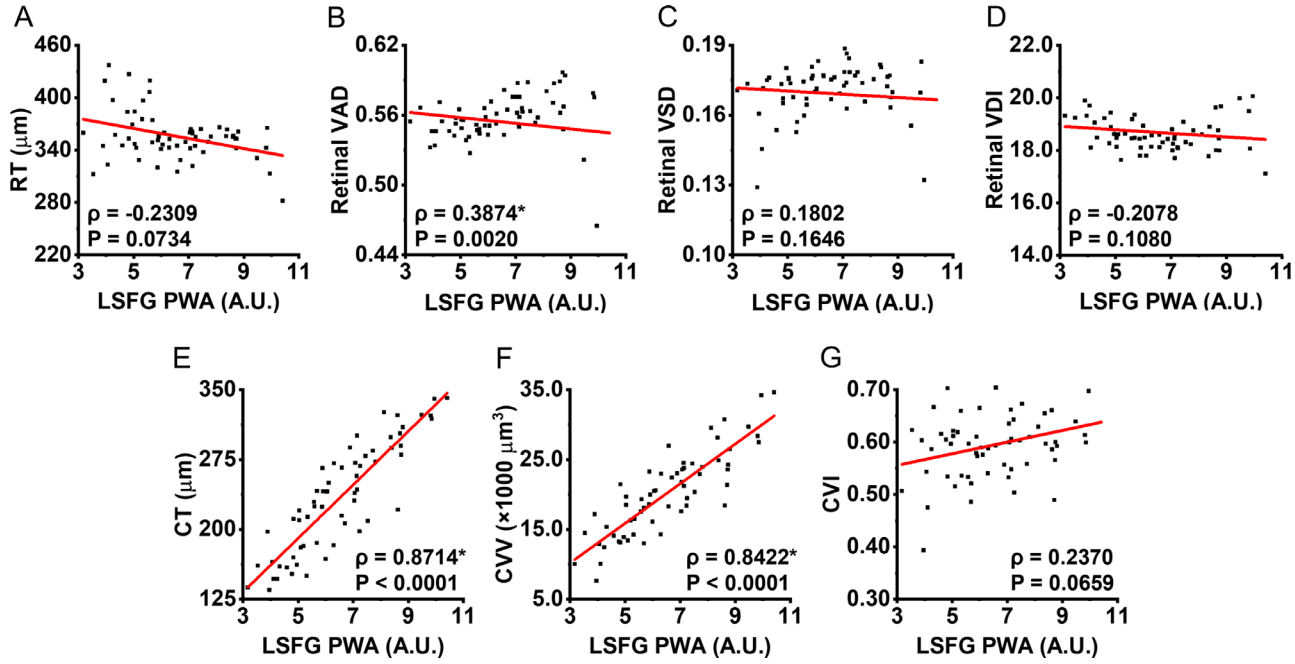

Figure 5. Representative correlations between the amplitude of the LSFG PWA and the OCT retinal and choroidal metrics. (A–D) Correlations between PWA and retinal thickness, VAD, VSD, VCI, VDI, and VPI. (E–G) Correlations between PWA and choroidal thickness, CVV, and CVI. The *red lines* represent the linear fitting of the scatters in each plot. Data were analyzed through Spearman's correlation analysis. Significance level was determined as $P < 0.05$.

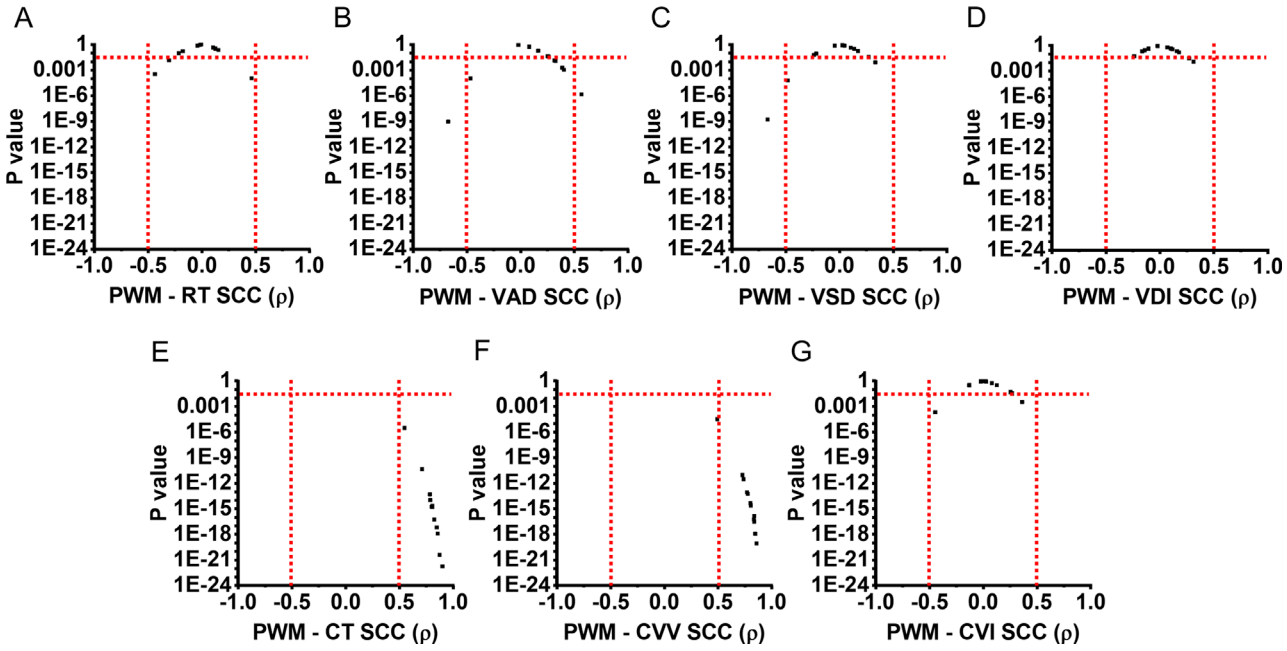

Figure 6. Correlation analysis between the LSFG PWM and retinal and choroidal metrics, obtained from 12 participants. Correlations between PWM and RT (A), VAD (B), VSD (C), VCI (D), VDI (E), VPI (F), CT (G), CVV (H), and CVI (I). The x- and y-axes represent Spearman's correlation coefficient and the *P* value. The *vertical red-dashed lines* represent $\rho = -0.5$ and 0.5 strength level of the correlation. The *horizontal red-dashed lines* illustrate the $P = 0.05$ significance level of the correlation. SCC, Spearman's correlation coefficient. *P* values are displayed on a logarithmic scale.

Similar correlation relationships were found between LSFG PWA and the OCT retinal and choroidal metrics. In most cases, PWA was weakly or not correlated with the retinal metrics (Figs. 7A–D). Eight of 12 cases showed ρ values larger than 0.5, with *P* values smaller than 0.05 in both the correlations of PWA – CT and PWA – CVV (Figs. 7E, 7F). All cases showed weak or no correlation between PWA and CVI

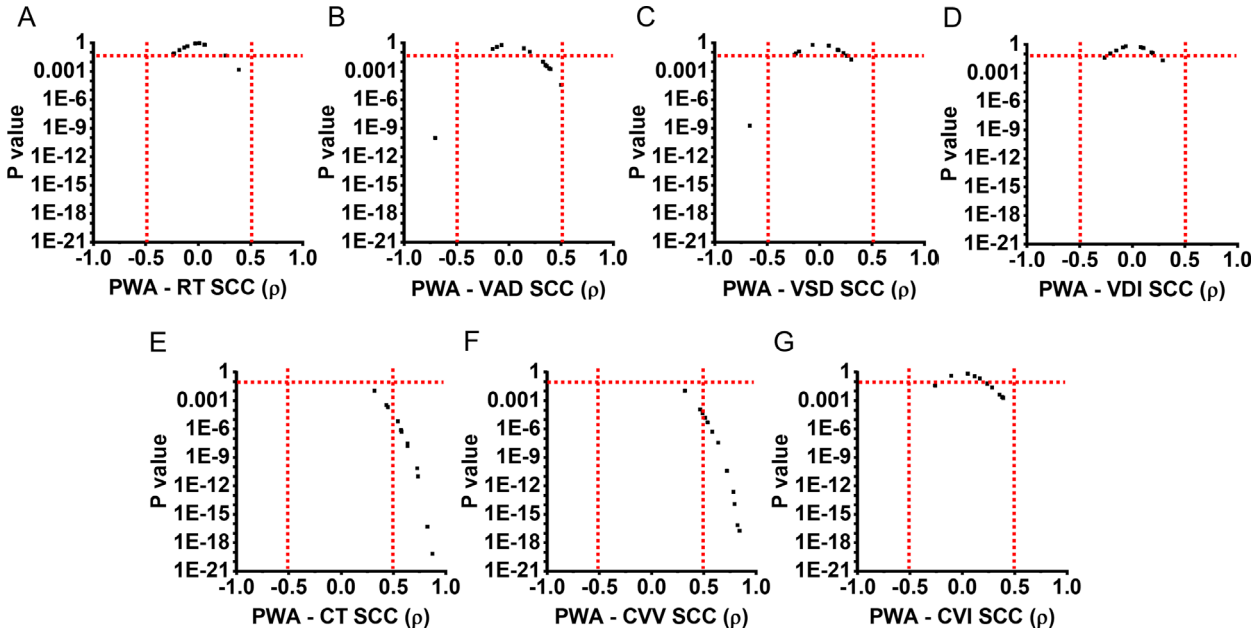

Figure 7. Correlation analysis between the LSFG PWA and retinal and choroidal metrics, obtained from 12 participants. Correlations between PWA and RT (A), VAD (B), VSD (C), VDI (D), CT (E), CVV (F), and CVI (G). The x- and y-axes represent Spearman's correlation coefficient and the *P* value, respectively. The *vertical red-dashed lines* represent the $\rho = -0.5$ and 0.5 strength level of the correlation. The *horizontal red-dashed lines* illustrate the $P = 0.05$ significance level of the correlation. *P* values are displayed on a logarithmic scale.

($-0.261 < \rho < 0.389$) (Fig. 7G). The results indicate that PWA was significantly correlated with CT and CVV but was weakly or not correlated with the retinal metrics and CVI.

Discussion

LSFG signals in the regions absent from large retinal vessels were investigated in this study. The background area in a LSFG map is defined as the locations where retinal vessels cannot be resolved. Due to the limitation of spatial resolution in the LSFG, only large blood vessels can be identified in the retina. Therefore, the background area includes all the rest regions, containing retinal capillaries, nonvessel tissue, choroidal vessels, and stroma. The background area in this study has a similar concept to the "tissue area" in some other LSFG studies, but with the emphasis that retinal capillaries and choroidal vessels are also presented in these regions.[33–35] Retinal capillaries can contribute to the background LSFG signals in certain ways, although they are barely resolved. In principle, the blood flows in the capillaries can decorrelate the speckles, although at a much lower level compared with those in the arteries or veins. This variation of speckles can be reflected as a general increase of the signal floor within a certain area without showing specific vessel morphology. For example, LSFG revealed postocclusive reactive hyperemia in forearms where blood vessels are unresolvable.[36] Similarly, blood flows in the choroidal vessel can also contribute to the background LSFG signals. However, the choroidal signals are vulnerable to the retinal signals due to choroid vessels being deeply beneath the retina. Therefore, the background LSFG signals can have multiple sources.

Two parameters regarding the LSFG, PWM and PWA, were employed in this study. PWM measured the averaged intensity and PWA measured the amplitude of the pulse waveform of the LSFG signals. Physiologically, PWM reflects the total blood volume that went through the sampling location during the recording period. In comparison, PWA correlates the pulse pressure, which is the difference between the systolic pressure and diastolic pressure. With the consideration that small vessels have weaker pulsations compared with the large vessels, PWM can also reflect more information about the flows in the small vessels, while PWA majorly represents the flows in the large vessels.[37,38] An important observation is the nonuniform spatial distribution (i.e., topography) of the LSFG signals in the background area. The topography of the LSFG signals was also different between individuals. Although it was not emphasized, the spatially variant topography of the LSFG signals has been observed in many previous studies.[16,39–42] Apparently, the background LSFG signals reflect the local blood flows, but this should not be simply attributed to either the retinal or choroidal signals without knowing the structural and vascular information about the retina and choroid.

To address this issue, OCT and OCTA were adopted in this study to provide metrics that separately depict the structural and vascular attributes of retina and choroid at a high spatial resolution. The results showed that both PWM and PWA were weakly or not correlated with the retinal metrics. In comparison, they were significantly correlated with CT and CVV. The strong correlation between CVV and the LSFG signals is straightforward since larger blood vessel volume corresponds to more blood flows that contribute to the LSFG signals. The significant correlation between CT and the LSFG signals may be attributed to the case that thicker choroid can contain more vessels. However, both PWM and PWA did not present a significant correlation with CVI, which reflected the volume density of the choroidal vessels in the choroidal tissue. Therefore, the results indicate that the LSFG signals in the background regions were dominated by the amount of blood flow in the choroid. Nevertheless, the results should not disprove the contribution of the retinal blood flows to the LSFG signals. In theory, blood flows in the unresolvable retinal capillaries can still decorrelate the laser speckle and contribute to the LSFG signals. In fact, in some cases, the retinal metrics presented weak correlations with PWM and PWA (Figs. 6, 7). Future works that use shorter wavelength lasers with limited penetration within the retina can further illustrate the retinal contribution to the LSFG signals.

There are limitations in this study. First, the OCT and OCTA metrics employed in this study quantified the geometrical attributes of the retinal and choroidal structure and vasculature, such as the thickness and density, instead of the real blood flow in the vessels. In principle, these metrics are associated with the blood flows since the flow attributes, such as flow velocity and resistance, are associated with the geometrical properties of the vessels.[37,38] Since there lacks a method to separately measure the flow in retina and choroid, we chose to use these OCT and OCTA metrics to represent the blood perfusions. Second, the identification of the large retinal vessels was based on the 6-mm × 6-mm en face OCTA images of the retina, using a custom-designed algorithm and a global threshold. The performance of the large vessel identification relied on the quality of the OCTA images and the

sensitivity limitation of the algorithm. Small portions of large vessels could be missed at some locations (arrowheads in Figs. 1C, 1F), but these missed vessels should not alter the general trend of the correlations as their overall area was relatively small compared with the vessel area that was successfully identified. Third, the size difference of the large retinal vessels in the LSFG and OCTA maps was not precisely calibrated. As a compromise, the vessel areas identified in the retinal OCTA maps were dilated by a certain number of pixels to generate the vessel mask that was then applied to other maps. The results showed that the large retinal vessels in the LSFG maps were reasonably removed (Fig. 1), but further efforts can still be spent on optimizing the large vessel mask to involve more background areas for analysis. The purpose of this study is to demonstrate the contribution of retinal and choroidal blood flows in the LSFG signals. Therefore, only healthy eyes were involved, and the influence of age was not considered. Moreover, the population number was also relatively small. Future studies with a larger population and age range, and patients with different diseases, such as DR, AMD, and glaucoma, are desirable to better illustrate the signal sources in LSFG and confirm its clinical significance.

In summary, the topographic correlations between the background LSFG signals and the retinal and choroidal structural and vascular metrics at the corresponding area were established in this study. Our results demonstrate that choroid flows dominate the LSFG signals at the areas without large retinal vessels and indicate that LSFG is a useful technique in the study of eye diseases that are correlated with choroidal blood perfusion abnormalities, such as AMD and central serous chorioretinopathy.

Acknowledgments

Supported in part by grants from the National Eye Institute (R01EY028753); an unrestricted grant from the Research to Prevent Blindness, Inc., New York, NY; and Washington Research Foundation. The funding organization had no role in the design or conduct of this research.

Disclosure: **Y. Lu**, None; **H. Zhou**, None; **X. Zhou**, None; **Y. Chen**, None; **R.K. Wang**, None

References

1. Linsenmeier RA, Padnick-Silver L. Metabolic dependence of photoreceptors on the choroid in the normal and detached retina. *Invest Ophthalmol Vis Sci*. 2000;41:3117–3123.
2. Nickla DL, Wallman J. The multifunctional choroid. *Prog Retin Eye Res*. 2010;29:144–168.
3. Langham ME, Grebe R, Hopkins S, Marcus S, Sebag M. Choroidal blood-flow in diabetic-retinopathy. *Exp Eye Res*. 1991;52:167–173.
4. Ciulla TA, Harris A, Kagemann L, et al. Choroidal perfusion perturbations in non-neovascular age related macular degeneration. *Br J Ophthalmol*. 2002;86:209–213.
5. Cherecheanu AP, Garhofer G, Schmidl D, Werkmeister R, Schmetterer L. Ocular perfusion pressure and ocular blood flow in glaucoma. *Curr Opin Pharmacol*. 2013;13:36–42.
6. Boas DA, Dunn AK. Laser speckle contrast imaging in biomedical optics. *J Biomed Opt*. 2010;15:011109.
7. Sugiyama T, Araie M, Riva CE, Schmetterer L, Orgul S. Use of laser speckle flowgraphy in ocular blood flow research. *Acta Ophthalmologica*. 2010;88:723–729.
8. Witkowska KJ, Bata AM, Calzetti G, et al. Optic nerve head and retinal blood flow regulation during isometric exercise as assessed with laser speckle flowgraphy. *PLoS One*. 2017;12:e0184772.
9. Calzetti G, Fondi K, Bata AM, et al. Assessment of choroidal blood flow using laser speckle flowgraphy. *Br J Ophthalmol*. 2018;102:1679–1683.
10. Shiga Y, Kunikata H, Aizawa N, et al. Optic nerve head blood flow, as measured by laser speckle flowgraphy, is significantly reduced in preperimetric glaucoma. *Curr Eye Res*. 2016;41:1447–1453.
11. Calzetti G, Mora P, Favilla S, et al. Assessment of choroidal neovascularization perfusion: a pilot study with laser speckle flowgraphy. *Translational Vision Science & Technology*. 2020;9:9.
12. Iwase T, Kobayashi M, Yamamoto K, Ra E, Terasaki H. Effects of photocoagulation on ocular blood flow in patients with severe non-proliferative diabetic retinopathy. *PLoS One*. 2017;12:e0174427.
13. Heeman W, Steenbergen W, van Dam G, Boerma EC. Clinical applications of laser speckle contrast imaging: a review. *J Biomed Opt*. 2019;24:1–11.
14. Shiga Y, Asano T, Kunikata H, et al. Relative flow volume, a novel blood flow index in the human retina derived from laser speckle flowgraphy. *Invest Ophthalmol Vis Sci*. 2014;55:3899–3904.
15. Isono H, Kishi S, Kimura Y, Hagiwara N, Konishi N, Fujii H. Observation of choroidal circulation using index of erythrocytic velocity. *Arch Ophthalmol*. 2003;121:225–231.

16. Kinoshita T, Mori J, Okuda N, et al. Effects of exercise on the structure and circulation of choroid in normal eyes. *PLoS One*. 2016;11:e0168336.
17. Saito M, Noda K, Saito W, Hirooka K, Hashimoto Y, Ishida S. Increased choroidal blood flow and choroidal thickness in patients with hypertensive chorioretinopathy. *Graef Arch Clin Exp*. 2020;258:233–240.
18. Chen CL, Wang RK. Optical coherence tomography based angiography [Invited]. *Biomed Opt Express*. 2017;8:1056–1082.
19. Chu Z, Lin J, Gao C, et al. Quantitative assessment of the retinal microvasculature using optical coherence tomography angiography. *J Biomed Opt*. 2016;21:66008.
20. Reif R, Qin J, An L, Zhi Z, Dziennis S, Wang R. Quantifying optical microangiography images obtained from a spectral domain optical coherence tomography system. *Int J Biomed Imaging*. 2012;2012:509783.
21. Ashimatey BS, Green KM, Chu ZD, Wang RKK, Kashani AH. Impaired retinal vascular reactivity in diabetic retinopathy as assessed by optical coherence tomography angiography. *Invest Ophthalmol Vis Sci*. 2019;60:2468–2473.
22. Choma M, Sarunic M, Yang C, Izatt J. Sensitivity advantage of swept source and Fourier domain optical coherence tomography. *Opt Express*. 2003;11:2183–2189.
23. Copete S, Flores-Moreno I, Montero JA, Duker JS, Ruiz-Moreno JM. Direct comparison of spectral-domain and swept-source OCT in the measurement of choroidal thickness in normal eyes. *Br J Ophthalmol*. 2014;98:334–338.
24. Zhang C, Tatham AJ, Medeiros FA, Zangwill LM, Yang Z, Weinreb RN. Assessment of choroidal thickness in healthy and glaucomatous eyes using swept source optical coherence tomography. *PLoS One*. 2014;9:e109683.
25. Zheng F, Gregori G, Schaal KB, et al. Choroidal thickness and choroidal vessel density in nonexudative age-related macular degeneration using swept-source optical coherence tomography imaging. *Invest Ophthalmol Vis Sci*. 2016;57:6256–6264.
26. Lains I, Talcott KE, Santos AR, et al. Choroidal thickness in diabetic retinopathy assessed with swept-source optical coherence tomography. *Retina*. 2018;38:173–182.
27. Zhou H, Chu Z, Zhang Q, et al. Attenuation correction assisted automatic segmentation for assessing choroidal thickness and vasculature with swept-source OCT. *Biomed Opt Express*. 2018;9:6067–6080.
28. Zhou H, Dai Y, Shi Y, et al. Age-related changes in choroidal thickness and the volume of vessels and stroma using swept-source oct and fully automated algorithms. *Ophthalmol Retina*. 2020;4:204–215.
29. Huang YP, Zhang QQ, Thorell MR, et al. Swept-source OCT angiography of the retinal vasculature using intensity differentiation-based optical microangiography algorithms. *Osli Retina*. 2014;45:382–389.
30. Lu YM, Wang RK. Removing dynamic distortions from laser speckle flowgraphy using Eigendecomposition and spatial filtering. *Journal of Biophotonics*. 2021;15:e202100294.
31. Vaz PG, Humeau-Heurtier A, Figueiras E, Correia C, Cardoso J. Laser speckle imaging to monitor microvascular blood flow: a review. *IEEE Rev Biomed Eng*. 2016;9:106–120.
32. Yan Y, Zhou X, Chu Z, et al. Vision loss in optic disc drusen correlates with increased macular vessel diameter and flux and reduced peripapillary vascular density. *Am J Ophthalmol*. 2020;218:214–224.
33. Kohmoto R, Sugiyama T, Ueki M, et al. Correlation between laser speckle flowgraphy and optical coherence tomography angiography measurements in normal and glaucomatous eyes. *Clin Ophthalmol*. 2019;13:1799–1805.
34. Takeyama A, Ishida K, Anraku A, Ishida M, Tomita G. Comparison of optical coherence tomography angiography and laser speckle flowgraphy for the diagnosis of normal-tension glaucoma. *J Ophthalmol*. 2018;2018:1751857.
35. Kiyota N, Kunikata H, Shiga Y, Omodaka K, Nakazawa T. Relationship between laser speckle flowgraphy and optical coherence tomography angiography measurements of ocular microcirculation. *Graef Arch Clin Exp*. 2017;255:1633–1642.
36. Alexandrou ME, Gkaliagkousi E, Loutradis C, et al. Haemodialysis and peritoneal dialysis patients have severely impaired post-occlusive skin forearm vasodilatory response assessed with laser speckle contrast imaging. *Clin Kidney J*. 2021;14:1419–1427.
37. Safar ME. Peripheral pulse pressure, large arteries, and microvessels. *Hypertension*. 2004;44:121–122.
38. Guven G, Hilty MP, Ince C. Microcirculation: physiology, pathophysiology, and clinical application. *Blood Purif*. 2020;49:143–150.
39. Saito W, Hashimoto Y, Hirooka K, Ishida S. Changes in choroidal blood flow velocity in patients diagnosed with central serous chorioretinopathy during follow-up for pachychoroid pigment epitheliopathy. *Am J Ophthalmol Case Rep*. 2020;18:100651.

40. Hashimoto R, Hirota A, Maeno T. Choroidal blood flow impairment demonstrated using laser speckle flowgraphy in a case of commotio retinae. *Am J Ophthalmol Case Rep*. 2016;4:30–34.
41. Hashimoto R, Kawamura J, Hirota A, Oyamada M, Sakai A, Maeno T. Changes in choroidal blood flow and choroidal thickness after treatment in two cases of pediatric anisohypermetropic amblyopia. *Am J Ophthalmol Case Rep*. 2017;8:39–43.
42. Calzetti G, Mora P, Borrelli E, et al. Short-term changes in retinal and choroidal relative flow volume after anti-VEGF treatment for neovascular age-related macular degeneration. *Sci Rep*. 2021;11:23723.